Chapter 34
Model Order Reduction of Nonlinear Euler-Bernoulli Beam

Shahab Ilbeigi and David Chelidze

Abstract Numerical simulations of large-scale models of complex systems are essential to modern research and development. However these simulations are also problematic by requiring excessive computational resources and large data storage. High fidelity reduced order models (ROMs) can be used to overcome these difficulties, but are hard to develop and test. A new framework for identifying subspaces suitable for ROM development has been recently proposed. This framework is based on two new concepts: (1) *dynamic consistency* which indicates how well does the ROM preserve the dynamical properties of the full-scale model; and (2) *subspace robustness* which indicates the suitability of ROM for a range of initial conditions, forcing amplitudes, and system parameters. This framework has been tested on relatively low-dimensional systems; however, its feasibility for more complex systems is still unexplored.

A 58 degree-of-freedom fixed-fixed nonlinear Euler-Bernoulli beam is studied, where large-amplitude forcing introduces geometrical nonlinearities. The responses of the beam subjected to both harmonic and random loads are obtained using finite difference method. The ROM subspaces are identified using the framework with both Proper Orthogonal Decomposition (POD) and Smooth Orthogonal Decomposition (SOD). POD- and SOD-based ROMs are then compared and fidelity of the new framework is evaluated.

Keywords Model order reduction • Dynamic consistency • Subspace robustness • Geometrical nonlinearity • Proper and smooth orthogonal decomposition

34.1 Introduction

Even with today's advances in computing technologies, long-time simulations of complex systems (e.g., molecular/multi-body/computational fluid dynamics, rationale drug template design or large-scale structural finite element models) are difficult. Such large- scale models can be unburdened of unnecessary computations using reduced order models (ROMs) [1]. However, not all ROMs are faithful. A faithful ROM is valid over a range of system parameters, initial conditions and input functions [1, 2].

There are different methods for model reduction of linear and nonlinear systems. For linear systems, these methods are well established. Such methods include Galerkin reduction using linear normal modes (LNMs) [3, 4] Krylov subspaces projection [5], and proper orthogonal decomposition (POD, also known as, singular value decomposition, principal component analysis, and Karhunen-Loeve Decomposition) [6–12]. However, in most cases the complexity of the system is caused by its nonlinearity. Many techniques are proposed for reduction of nonlinear models. These techniques include, but are not limited to, inertial manifold approximation, linearization about the equilibrium point [13, 14], center manifold theory [15, 16], nonlinear normal modes (NNMs) [17–20], and POD.

Commonly used methodologies for model reduction of nonlinear systems can be categorized in two groups. In the first method, the nonlinear manifold is approximated using NNMs [17–20]. Although the nonlinear manifold has the lowest dimension needed, it is limited with the difficulty of the analytical calculations used in the approximation. Besides, the nonlinear manifold identified for a given energy may be different for other energy levels [1].

In the second method, the nonlinear system can be projected onto a linear subspace spanned by a set of appropriate basis functions [6, 11]. These bases can be identified by proper orthogonal modes (POMs) and smooth orthogonal modes (SOMs) in POD and SOD methods, respectively. By definition, POMs are limited to be orthogonal; hence, they capture the nonlinear manifold by a higher dimensional linear subspace than SOMs [1]. Furthermore, in contrast to POD, SOD considers

S. Ilbeigi • D. Chelidze (✉)
Department of Mechanical, Industrial and Systems Engineering, University of Rhode Island, Kingston, RI 02881, USA
e-mail: chelidze@egr.uri.edu

G. Kerschen (ed.), *Nonlinear Dynamics, Volume 1*, Conference Proceedings of the Society for Experimental Mechanics Series, DOI 10.1007/978-3-319-15221-9_34

both spatial and temporal characteristics of the data set. In particular, SOD identifies coordinates (smooth orthogonal coordinates- or SOCs) that have both minimal temporal roughness and maximal spatial variance. Therefore, SOD obtains the smoothest low dimensional approximation of a high dimensional system.

The fidelity of a ROM can be investigated by raising two questions: (1) "How well does it approximate the full-scale system?" and (2) "Is it valid over a wide range of system's level of energy?" A recently developed framework [1, 2] addresses these questions. This framework is based on two concepts: dynamical consistency and subspace robustness. These concepts were used to estimate the lowest dimensional subspaces suitable for ROM for both POD and SOD. It was shown that using SOD, the dynamics of a nonlinear system can be captured in a lower dimensional ROM. However, the studied system was relatively low-dimensional and thus the fidelity of the framework as well as the performance of the SOD are needed to be explored for more complex nonlinear systems.

To this aim, a nonlinear Euler-Bernoulli beam is modeled based on the explicit finite difference scheme. The geometrically nonlinear regime, which governs this system, has an interesting full-scale model solution with high-amplitude transverse and low-amplitude axial vibrations. Thus, its full state-space model is a combination of coordinates having very low and high variances. The ability of the POD in capturing the dynamics of this system is in question since it only looks at these variances. Using the new framework, the ROM subspaces are identified for both POD and SOD and their performances are contrasted. Prior to doing that, a brief review on nonlinear model reduction theory, dynamical consistency and subspace robustness is provided.

34.2 Nonlinear Model Reduction

Full-scale model of a deterministic dynamical system has the following form:

$$\dot{y} = f\,(y, t) \tag{34.1}$$

where $y \in \mathbb{R}^n$ is a dynamic state variable, $f : \mathbb{R}^n \times \mathbb{R} \to \mathbb{R}^n$ is some nonlinear flow, $t \in \mathbb{R}$ is time, and $n \in \mathbb{N}$ is usually twice the number of the system's degrees-of-freedom. The state variable trajectories data can be arranged in the matrix $Y = [y_1,\ y_2,\ \ldots,\ y_n] \in \mathbb{R}^{m \times n}$. A basis for Y can be calculated using either POD or SOD using the procedure explained in [1]. These most dominant k-dimensional bases are arranged in the matrix $P_k = [e_1,\ e_1, \ldots,\ e_k]$. Now, using a coordinate transformation of $q = P_k\ Y \in \mathbb{R}^n$ to give the reduced state variable, the corresponding ROM is:

$$\dot{q} = P_k^{\dagger} f\,(P_k\ q, t) \tag{34.2}$$

where $(.)^{\dagger}$ indicates the pseudoinverse of (.).

34.3 Model Reduction Subspace Selection

The appropriate subspace for model reduction can be selected based on a newly developed criterion [1]. This criterion quantifies two concepts: dynamical consistency – which demonstrates how well the linear subspace embeds the nonlinear manifold – and subspace robustness –which explains the sensitivity of the subspace to changes in system's level of energy. Here, these concepts are briefly reviewed. A more complete description can be found in [1].

34.3.1 Dynamical Consistency

The idea behind dynamical consistency is based on the unfolding of an attractor used in delay coordinate embedding [21] and can be determined by the premise behind a method of false nearest neighbors [22]. A linear subspace used for model reduction is said to be dynamically consistent if the resultant trajectories are deterministic and smooth. The metric for dynamical consistency is defined as the ratio of the number of false nearest neighbors (FNN) over the total number of nearest neighbor pairs in a particular k-dimensional subspace:

$$\zeta^k = 1 - \frac{N_{fnn}^k}{N_{nn}} \tag{34.3}$$

where N_{fnn}^{k} is the estimated number of FNNs in k-dimensional subspace, and N_{nn} is the total number of nearest neighbor pairs used in the estimation. If ζ^{k} is close to unity, then that k-dimensional subspace is dynamically consistent.

34.3.2 Subspace Robustness

Unlike linear normal mode subspaces that are unique and insensitive to the level of energy, the robustness of the subspaces obtained by data analysis methods should be determined. In order to quantify the subspace robustness, the basis vectors, which span the k-dimensional subspace for s systems with different level of energy, form a matrix $\mathbf{S} \in \mathbb{R}^{n \times ks}$. Then, the corresponding subspace robustness γ_{s}^{k} is given by the following expression:

$$\gamma_{s}^{k} = \left| 1 - \frac{4}{\pi} \arctan \sqrt{\frac{\sum_{i=k+1}^{n} \sigma_{i}^{2}}{\sum_{i=1}^{k} \sigma_{i}^{2}}} \right| \tag{34.4}$$

where σ_{i} ' s are proper orthogonal values of the matrix $\mathbf{S}$.

34.4 Nonlinear Euler-Bernoulli Beam

In this work, a ROM for vibrations of a high-dimensional nonlinear Euler-Bernoulli beam is investigated. A physical beam model is shown in Fig. 34.1. The mathematical model of this system is described in classical books devoted to spatial objects dynamics [23, 24]; here only the governing differential equations are given:

$$\begin{aligned} &\rho A \frac{\partial^2 u}{\partial t^2} + d_2 \frac{\partial u}{\partial t} - EA \left(\frac{\partial^2 u}{\partial x^2} + \frac{\partial w}{\partial x} \frac{\partial^2 w}{\partial x^2} \right) = 0 \\ &\rho A \frac{\partial^2 w}{\partial t^2} + EI \frac{\partial^4 w}{\partial x^4} + d_1 \frac{\partial w}{\partial t} - EA \left(\frac{\partial u}{\partial x} \frac{\partial^2 w}{\partial x^2} + \frac{\partial^2 u}{\partial x^2} \frac{\partial w}{\partial x} + \frac{3}{2} \frac{\partial^2 w}{\partial x^2} \left(\frac{\partial w}{\partial x} \right)^2 \right) = q\,(x,\ t)\,, \end{aligned} \tag{34.5}$$

where ρ is viscosity, E is Young's modulus of elasticity, A is the area of beam section, I is moment of inertia, d_1 and d_2 are damping coefficients, and $q(x, t)$ is transverse forcing. Also, $u(x, t)$ and $w(x, t)$ denote for axial and transverse vibrations, respectively. The beam under investigation is fixed-fixed at its ends with the following boundary conditions that are attached to Eq. (34.5):

$$w\,(0,\ t) = w\,(a,\ t) = u\,(0,\ t) = u\,(a,\ t) = \left. \frac{\partial w\,(x,\ t)}{\partial x} \right|_{x=0} = \left. \frac{\partial w\,(x,\ t)}{\partial x} \right|_{x=a} = 0 \tag{34.6}$$

In this case, both transverse and longitudinal displacements at beam's ends, as well as tangents to the slope at its ends are equal to zero. Besides, the following initial conditions are considered for the beam:

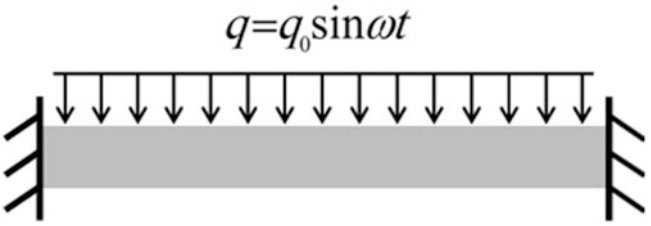

Fig. 34.1 Model of the nonlinear Euler-Bernoulli beam

$$
\begin{aligned}
w(x,\ t) &= w_0(x,\ t) \\
u(x,\ t) &= u_0(x,\ t) \\
\frac{\partial w(x,\ t)}{\partial t} &= \dot{w}_0(x,\ t) \\
\frac{\partial u(x,\ t)}{\partial t} &= \dot{u}_0(x,\ t)
\end{aligned}
\tag{34.7}
$$

For small transverse vibrations, the two equations given in Eq. (34.5) reduce to one linear equation, which only accounts for transverse vibrations. In that case, axial vibrations are very small and negligible. For large deflections, axial displacements are taken into account, which introduces geometrical nonlinearity to the system. There is no exact analytical solution for the nonlinear system; however, a finite-dimensional model of the system can be solved numerically using finite difference method. The method is described in next section.

34.4.1 Full-Dimensional System Model

The full-dimensional state-space model of the system in matrix form can be obtained using FDM. The space coordinate of the beam, as shown in Fig. 34.2, is meshed using $M + 2$ nodes. The parameters u_i and w_i indicate axial and transverse displacements of the i-th node. The space derivatives in Eq. (34.5) are substituted by their second order finite difference approximation $O(\Delta x^2)$ which are given as follows:

$$
\begin{aligned}
&\frac{\partial u}{\partial x} = \frac{u_{i+1} - u_{i-1}}{2\ \Delta x},\ \frac{\partial^2 u}{\partial x^2} = \frac{u_{i+1} - 2u_i + u_{i-1}}{\Delta x^2},\ \frac{\partial w}{\partial x} = \frac{w_{i+1} - w_{i-1}}{2\ \Delta x},\ \frac{\partial^2 w}{\partial x^2} = \frac{w_{i+1} - 2w_i + w_{i-1}}{\Delta x^2}, \\
&\frac{\partial^4 w}{\partial x^4} = \frac{w_{i+2} - 4w_{i+1} + 6w_i - 4w_{i-1} - w_{i-2}}{\Delta x^4},
\end{aligned}
\tag{34.8}
$$

where Δx is space mesh size. After simplifying, this leads to the following systems of ordinary differential equations:

$$
\begin{cases}
\ddot{w}_i + \alpha\ \dot{w}_i = H_i(x,t) \\
\ddot{u}_i + \beta\ \dot{u}_i = G_i(x,t)
\end{cases}
\quad \text{for } i = 1,\ 2,\ \ldots,\ M,
\tag{34.9}
$$

where $\alpha = \frac{d_1}{\rho A}$ and $\beta = \frac{d_2}{\rho A}$.

The boundary and initial conditions can be treated using two fictitious space layers, which are illustrated in Fig. 34.2. Therefore, using finite difference approximation one obtain:

$$
w_i(0) = w_{i0};\ \dot{w}_i(0) = \dot{w}_{i0};\ u_i(0) = u_{i0};\ \dot{u}_i(0) = \dot{u}_{i0}.
\tag{34.10}
$$

By introducing $y_i = w_i,\ y_{M+i} = u_i,\ y_{2M+i} = \dot{w}_i$ for $i = 1, \ldots, M$, the system can be written as $4M$-dimensional first-order equation in $y = \left[w_i\ u_i\ \dot{w}_i\ \dot{u}_i \right]^T \in \mathbb{R}^n,\ n = 4M$ as:

$$
\dot{\mathbf{y}} = \mathbf{A}\mathbf{y} + \mathbf{f}(y,t)
\tag{34.11}
$$

where $\mathbf{f}(y,t) = \left[\mathbf{0}_{1\times 2M}\ H_1(x,y,t)\ \ldots\ H_M(x,y,t)\ G_1(x,y,t)\ \ldots\ G_M(x,y,t) \right]^T \in \mathbb{R}^n$ and $\mathbf{A} = \begin{bmatrix} \mathbf{0}\ \mathbf{0} & \mathbf{I} & \mathbf{0} \\ \mathbf{0}\ \mathbf{0} & \mathbf{0} & \mathbf{I} \\ \mathbf{0}\ \mathbf{0} & -\alpha\mathbf{I} & \mathbf{0} \\ \mathbf{0}\ \mathbf{0} & \mathbf{0} & -\beta\mathbf{I} \end{bmatrix}$,

where $\mathbf{0} \in \mathbb{R}^{M\times M}$ is a zero matrix and $\mathbf{I} \in \mathbb{R}^{M\times M}$ is an identity matrix.

Equation (34.11) represents the full-dimensional mathematical model of the system. It is solved via Adams-Bashforth method with the accuracy of $O(\Delta t^4)$, where Δt is the time step. The matrix form of POD-based ROM or SOD-based ROM can be expressed as:

$$
\dot{\mathbf{q}} = \mathbf{P}_k{}^T \mathbf{A}\ \mathbf{P}_k\ \mathbf{q} + \mathbf{P}_k{}^T \mathbf{f}(y,t)
\tag{34.12}
$$

where $\mathbf{P}_k$ could be the most dominant k-dimensional POMs or the most dominant k-dimensional SOMs.

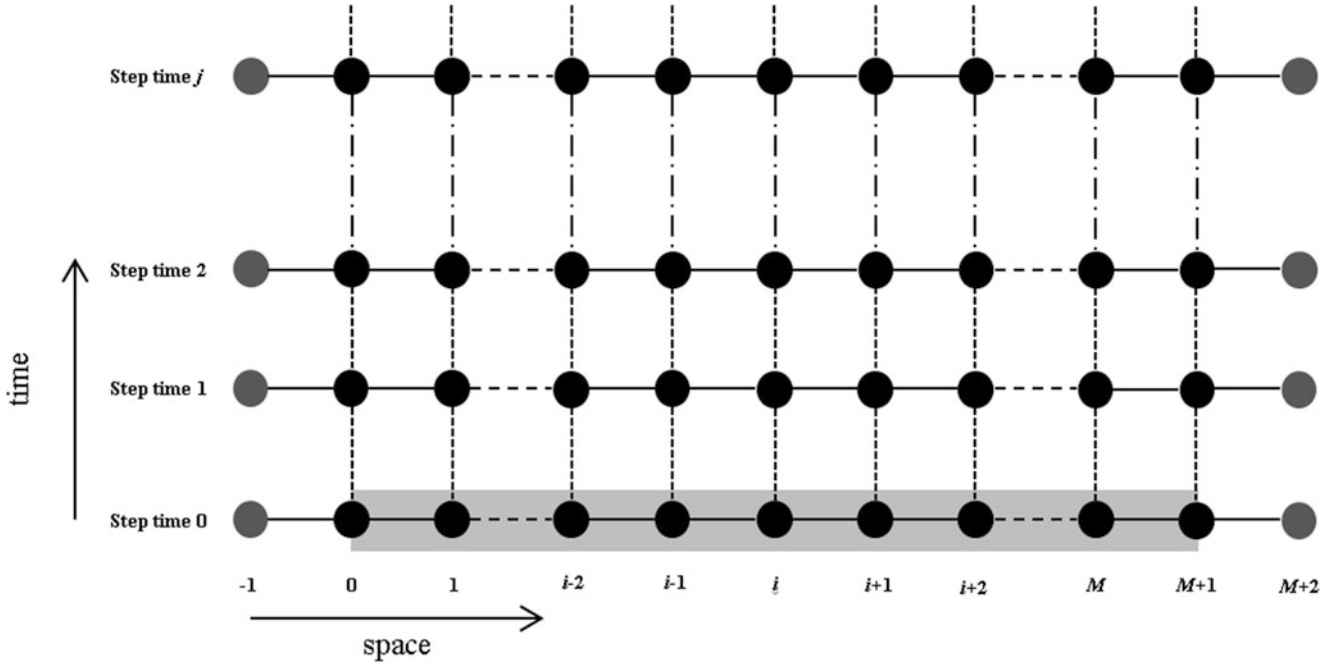

Fig. 34.2 Numerical scheme

34.5 Results and Discussion

34.5.1 Full-Dimensional Model

The space coordinate of the beam is meshed using $M = 29$ nodes. Thus, the full state space model is 116-dimensional, which means that 116 equations are needed to be solved simultaneously. The beam is assumed to be made of aluminum with density $\rho = 2710\ \text{kg/m}^3$, Young's Modulus $E = 69$ Gpa, dissipation ratios $\alpha = 1.845$ and $\beta = 0$. The beam's dimensions are $0.01\ \text{m} \times 0.01\ \text{m} \times 1\ \text{m}$. A harmonic transverse force $q = q_0 \sin \omega t$ is applied to the beam. For forcing frequency $\omega = 200$ Hz, and the parameter q_0 is used as a bifurcation parameter. The bifurcation diagram for the transverse vibrations of the beam's middle point is shown in Fig. 34.3. To obtain this diagram, the first 200 cycles of harmonic forcing are not used to eliminate transient. The next 200 cycles are then used in the calculations. The bifurcation diagram starts at $q_0 = 1$ with zero initial conditions. As the amplitude of forcing increases, new trajectories follow the previous solutions. A rich dynamical behavior, which includes chaotic response, can be observed in Fig. 34.3. For instance, the solution (transverse vibrations of the middle point) for some values of q_0 obtained using the full-dimensional model is depicted in Fig. 34.4.

The axial vibration of the most far end nodes has larger magnitude than other nodes. The phase space portrait of the most far left node, for the same values as in Fig. 34.4, are depicted in Fig. 34.5. It can be seen that their magnitudes are much smaller than those of the transverse vibrations. Therefore, the full-dimensional state space vector space has big variances in the coordinates corresponding to the transverse vibrations, but small variances for those corresponding to axial vibrations. POD-based MOR only considers the variances in configuration space while SOD-based MOR not only considers the spatial variances but also looks at the temporal characteristics of the trajectories in the full-dimensional state-space model. Thus, the authors expect SOD to capture the dynamic of the system in a lower-dimensional subspace. In next section, the results of both POD-and SOD-based MOR are discussed.

34.5.2 Reduced Order Model

To identify the modal structure using both POD and SOD, the beam is excited for a comparably long time by an appropriately filtered random forcing. This guarantees that nearly all the state space is explored and all dominant frequencies of the beam are covered. A set of 30 randomly driven trajectory data is used to estimate the subspaces robustness using the

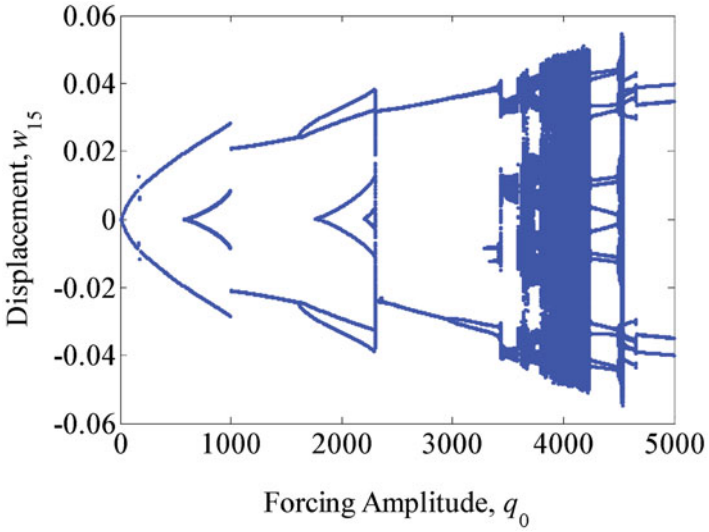

Fig. 34.3 Bifurcation diagram

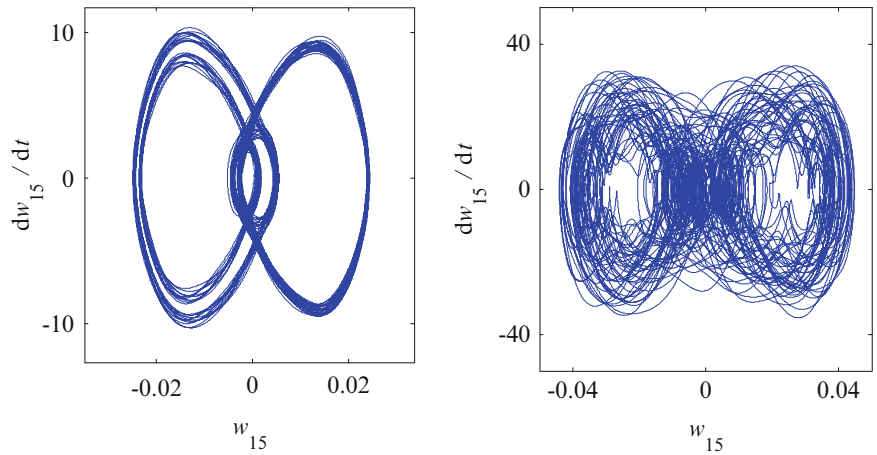

Fig. 34.4 transverse vibrations of the middle of beam: $q_0 = 760$ (*left*), $q_0 = 3900$ (*right*)

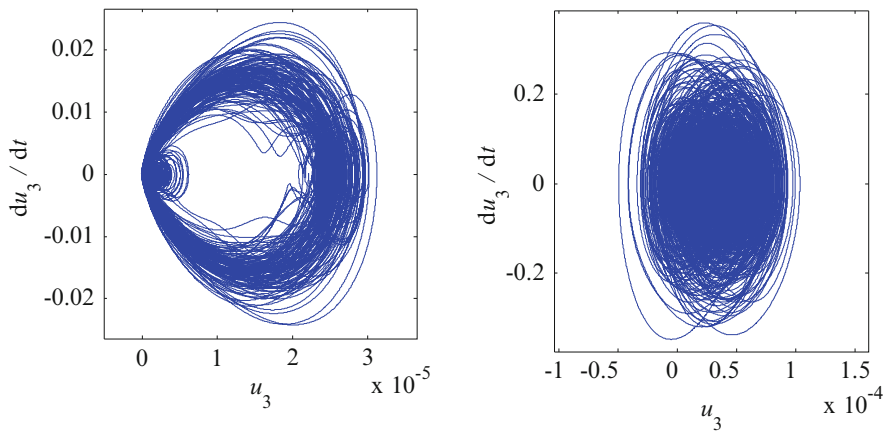

Fig. 34.5 axial vibrations of the most far left node on the beam: $q_0 = 760$ (*left*), $q_0 = 3900$ (*right*)

aforementioned procedure. Figure 34.6 illustrates the subspace robustness for all k-dimensional subspaces of the full-scale model. Each quantity in this figure gives a measure of sensitivity of its corresponding k-dimensional subspace to different forcing conditions. According to this figure, for $k \geq 13$, SOD subspace robustness is close to unity. The POD subspace robustness is not monotonic. It reaches unity at $k = 58$, however, suddenly drops by increasing the number of the modes.

The dynamical consistency is shown in Fig. 34.7 for both POD- and SOD-based ROMs. To estimate the dynamical consistency, the k-dimensional subspaces obtained from randomly driven data are used to project full dimensional space

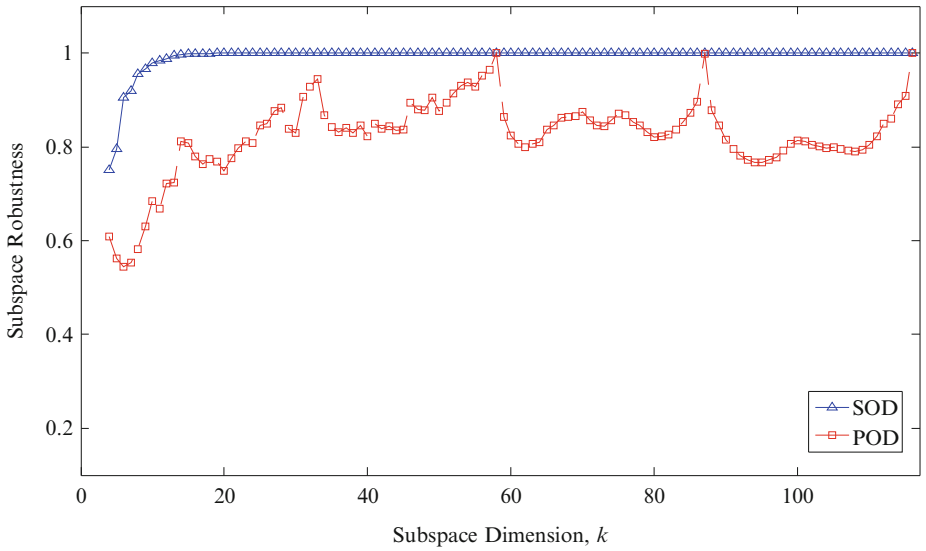

Fig. 34.6 Subspace robustness for randomly driven system

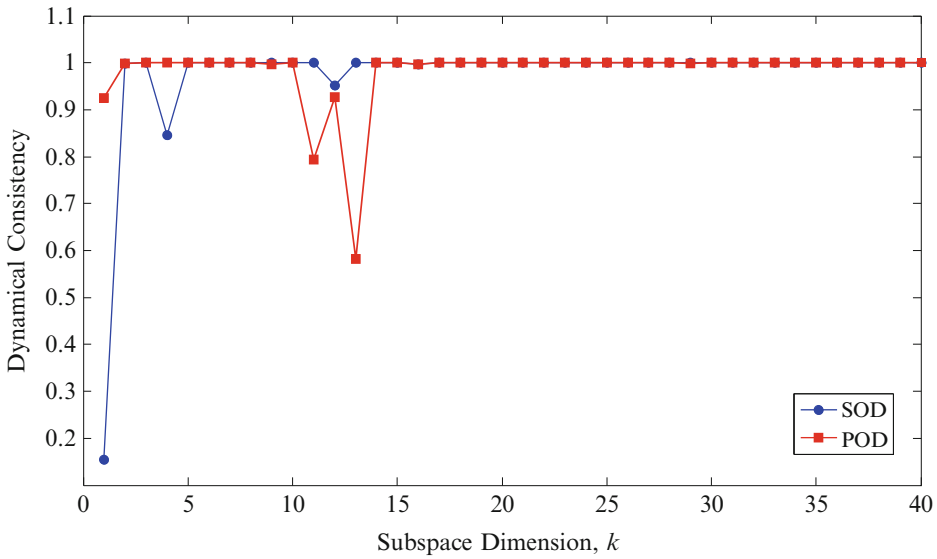

Fig. 34.7 Dynamical consistency

of harmonic data. This figure demonstrates that results for dynamical consistency of POD and SOD are similar, except for $k = 4,\ 11$ and 13, where POD subspaces are more consistent.

Now, the extracted modes can be used for building the POD- and SOD-based ROMs to simulate the solution of the full-scale model under harmonic forcing. The lowest dimensional SOD-based ROM, which is stable, has the dimension 47. Figure 34.8 depicts the results for POD- and SOD-based ROMs for harmonic forcing with $q_0 = 10$. Comparison with the full-scale model trajectories shows that POD-based ROM is not stable. To get a stable POD-based ROM, it has to be at least 65-dimensional.

In Fig. 34.9, the POD- and SOD-based ROM, obtained for a range of forcing amplitudes, are compared to full-scale model trajectories. It can be seen that SOD-based ROMs capture dynamic in a lower dimension. A 49-dimensional SOD-based ROM is able to reproduce good results while POD-based ROM needs at least 65 dimensions for that. POD-based ROM with dimension lower than 65 are not stable. Some SOD-based ROM with dimension lower than 49 had fairly good correlation with the full-scale model, however, failed after very few cycles of harmonic forcing.

The instability of lower dimensional ROMs is most likely to be due to the explicit nature of the FDM, which was used for solving both full-scale and reduced order models. However, another possibility, which could explain this problem, is the weak coupling between axial and transverse displacement of the nodes. This results in small magnitude of the data corresponding to state variables of the axial nodes in the full dimensional state space. Therefore, it might be difficult for both POD and SOD to identify the corresponding subspaces of these data properly. Nevertheless, SOD was shown to have a better performance in identifying these subspaces.

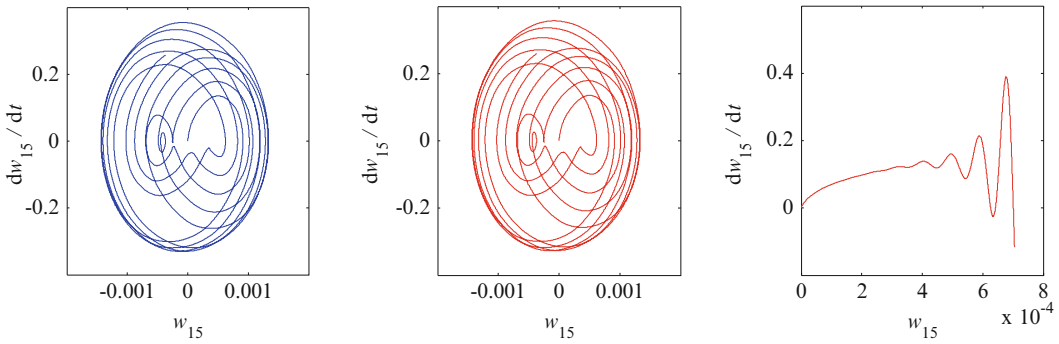

Fig. 34.8 Full-scale and ROM trajectories for periodic loading with $q_0 = 10$ and $\omega = 200$ Hz; Full-scale model (*left*), random SOD- based ROM (*middle*), random POD- based ROM (*right*)

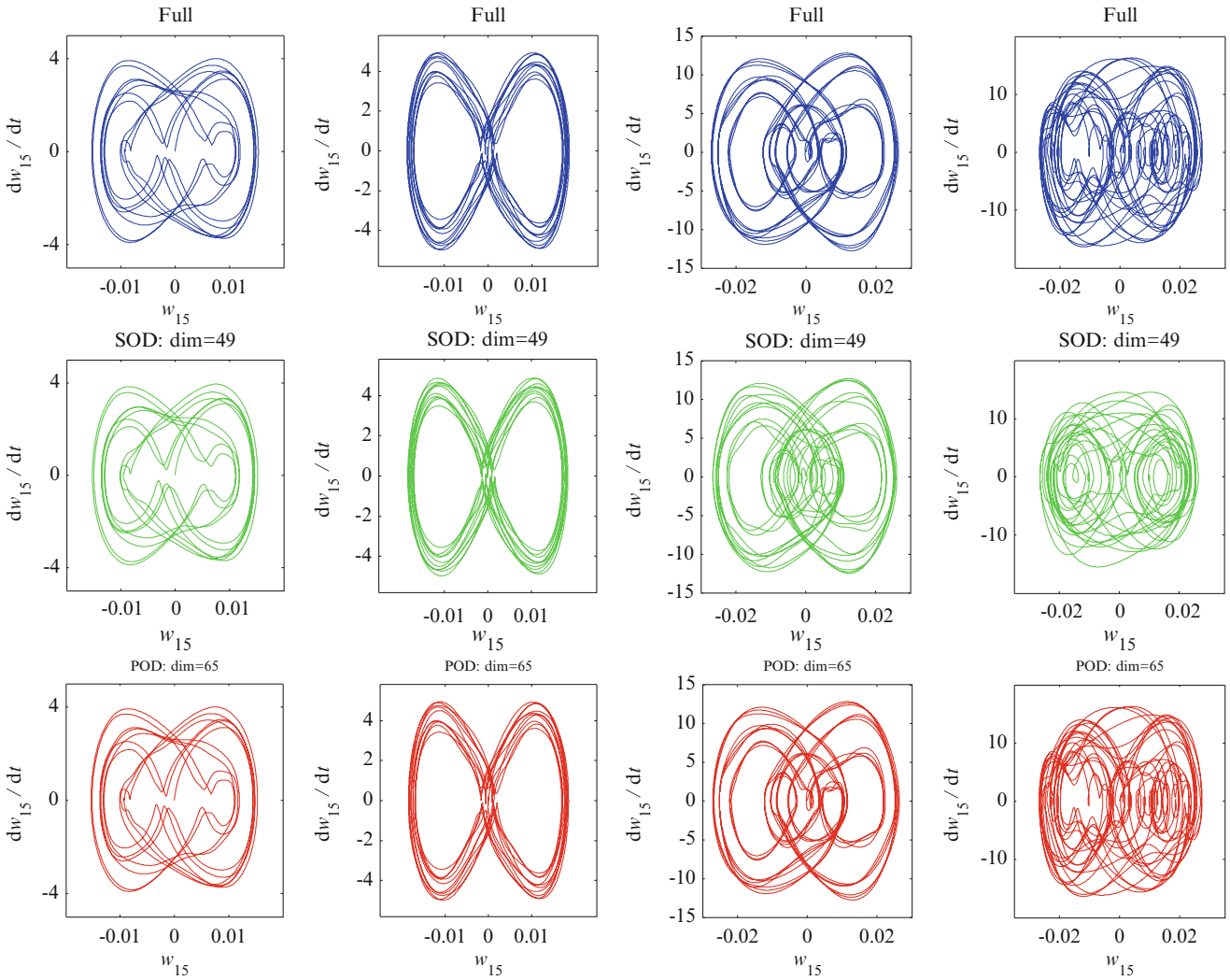

Fig. 34.9 POD- and SOD-based ROMs for $\omega = 200$ Hz and different forcing amplitudes: $f = 300$ (column 1), $f = 500$ (column 2), $f = 800$ (column 3) and $f = 1000$ (column 4)

34.6 Conclusion

The full state-space model of a nonlinear Euler-Bernoulli beam was obtained using FDM. POD and SOD subspaces for this system were obtained and their dynamical consistency and subspace robustness were evaluated. SOD subspaces were shown to be more robust than those of POD. Obtained subspaces were also used for building the ROMs of the system. ROM simulations showed that SOD-based ROM captures the dynamic of the full-scale system in a relatively lower dimensional space.

Although SOD had a better performance than POD, our effort for obtaining lower dimensional models failed. As discussed, that could be due to either instability of the advised numerical scheme or incapability of both POD and SOD. This problem should be addressed with different systems, where couplings between different coordinates are weak while either an analytical-based numerical method or implicit numerical scheme is available. This system would have geometric nonlinearity and its model can be solved using implicit methods. An example of such a system is a grid of masses, connected by springs and dampers, with two degree of freedom for each mass.

Acknowledgement The authors would like to thank National Science Foundation under Grant No. 1100031.

References

1. Chelidze D (2014) Identifying robust subspaces for dynamically consistent reduced-order models. Nonlinear Dyn 2:123–130
2. Segala DB, Chelidze D (2013) Robust and dynamically consistent reduced order models. In: ASME 2013 international mechanical engineering congress and exposition. American Society of Mechanical Engineers, pp V04BT04A010–V04BT04A010
3. Foias C, Jolly MS, Kevrekidis IG, Sell GR, Titi ES (1988) On the computation of inertial manifolds. Phys Lett A 131(7):433–436
4. Pesheck E, Pierre C, Shaw SW (2002) A new Galerkin-based approach for accurate non-linear normal modes through invariant manifolds. J Sound Vib 249(5):971–993
5. Feldmann P, Freund RW (1995) Efficient linear circuit analysis by Padé approximation via the Lanczos process. Comput Aid Des Integr Circuit Syst 14(5):639–649
6. Amabili M, Sarkar A, Paıdoussis MP (2003) Reduced-order models for nonlinear vibrations of cylindrical shells via the proper orthogonal decomposition method. J Fluids Struct 18(2):227–250
7. Georgiou I (2005) Advanced proper orthogonal decomposition tools: using reduced order models to identify normal modes of vibration and slow invariant manifolds in the dynamics of planar nonlinear rods. Nonlinear Dyn 41(1–3):69–110
8. Hall K, Thomas J, Dowell E (1999) Reduced-order modelling of unsteady small-disturbance flows using a frequency-domain proper orthogonal decomposition technique. In 37th Aerospace Science Meeting and Exhibit, no. AIAA Paper 99-0655
9. Kerschen G, Golinval JC, Vakakis AF, Bergman LA (2005) The method of proper orthogonal decomposition for dynamical characterization and order reduction of mechanical systems: an overview. Nonlinear Dyn 41(1–3):147–169
10. Rathinam M, Petzold LR (2003) A new look at proper orthogonal decomposition. SIAM J Numer Anal 41(5):1893–1925
11. Smith TR, Moehlis J, Holmes P (2005) Low-dimensional modeling of turbulence using the proper orthogonal decomposition: a tutorial. Nonlinear Dyn 41(1–3):275–307
12. Willcox K, Peraire J (2002) Balanced model reduction via the proper orthogonal decomposition. AIAA J 40(11):2323–2330
13. Phillips JR (2003) Projection-based approaches for model reduction of weakly nonlinear, time-varying systems. IEEE Trans Comput Aid Design Integr Circuits Syst 22(2):171–187
14. Bai Z (2002) Krylov subspace techniques for reduced-order modeling of large-scale dynamical systems. Appl Num Math 43(1):9–44
15. Carr J (1981) Applications of centre manifold theory. Springer-Verlag
16. Guckenheimer J, Holmes P (1983) Nonlinear oscillations, dynamical systems, and bifurcations of vector fields, vol 42. Springer, New York
17. Shaw S, Pierre C (1991) Non-linear normal modes and invariant manifolds. J Sound Vib 150(1):170–173
18. Shaw SW, Pierre C (1993) Normal modes for non-linear vibratory systems. J Sound Vib 164(1):85–124
19. Shaw SW, Pierre C (1994) Normal modes of vibration for non-linear continuous systems. J Sound Vib 169(3):319–347
20. Vakakis AF (1997) Non-linear normal modes (NNMs) and their applications in vibration theory: an overview. Mech Syst Signal Process 11(1):3–22
21. Sauer T, Yorke JA, Casdagli M (1991) Embedology. J Stat Phys 65(3–4):579–616
22. Kennel MB, Brown R, Abarbanel HD (1992) Determining embedding dimension for phase-space reconstruction using a geometrical construction. Phys Rev A 45(6):3403
23. Volmir AS (1974) The nonlinear dynamics of plates and shells. No FTD-HC-23-851-74. Foreign Technology DIV Wright-Patterson AFB OH
24. Virgin LN (2007) Vibration of axially loaded structures, 393rd edn. Cambridge University Press, New York